

Scratch that! An Evolution-based Adversarial Attack against Neural Networks

Malhar Jere, Farinaz Koushanfar
University of California San Diego
9500 Gilman Drive, La Jolla, CA
Email: mjere@ucsd.edu

Briland Hitaj, Gabriela Ciocarlie
SRI International
60 E 42nd St, New York
Email: briland.hitaj@sri.com, gabriela.ciocarlie@sri.com

Abstract—Recent research has shown that Deep Neural Networks (DNNs) for image classification are vulnerable to adversarial attacks. However, most works on adversarial samples utilize sub-perceptual noise that, while invisible or slightly visible to humans, often covers the entire image. Additionally, most of these attacks often require knowledge of the neural network architecture and its parameters, and the ability to calculate the gradients of the parameters with respect to the inputs. In this work, we show that it is possible to attack neural networks in a highly restricted threat setting, where attackers have no knowledge of the neural network (i.e., in a black-box setting) and can only modify highly localized adversarial noise in the form of randomly chosen straight lines or *scratches*. Our *adversarial scratches* attack method covers only 1-2% of the image pixels and are generated using the Covariance Matrix Adaptation Evolutionary Strategy, a purely black-box method that does not require knowledge of the neural network architecture and its gradients. Against ImageNet models, *Adversarial Scratches* requires 3 times fewer queries than GenAttack [2] (without any optimizations) and 73 times fewer queries than ZOO [11], both prior state-of-the-art black-box attacks. We successfully deceive state-of-the-art Inception-v3 [53], ResNet-50 [22] and VGG-19 [51] models trained on ImageNet with deceiving rates of 75.8%, 62.7%, and 45% respectively, with fewer queries than several state-of-the-art black-box attacks, while modifying less than 2% of the image pixels. Additionally, we provide a new threat scenario for neural networks, demonstrate a new attack surface that can be used to perform adversarial attacks, and discuss its potential implications.

I. INTRODUCTION

Deep Neural Networks (DNNs) have achieved state-of-the-art results in image classification [22], [23], [28], [51], [53], machine translation [13], [14], [41] and reinforcement learning tasks [5], [49], [50], [57], and are being applied to a wide variety of domains, such as cancer detection from medical scans [1], [48], malware detection [30], [42], [56], speech recognition [20], and more. However, despite these accomplishments, they are also susceptible to being deceived by adversarial inputs, which consist of images containing sub-perceptual noise invisible to humans that can make a neural network misclassify an input to any potential target. Such adversarial samples can be targeted to misclassify to a chosen class, or untargeted, where the misclassification can be to any class that is not ground truth. Researchers have demonstrated that adversarial samples transfer to the real-world can be printed on paper or on 3D-models [4], and can exist for classifiers for multiple modalities, such as

images [54], speech [9], and text [3]. Beyond the security threats that adversarial samples pose to neural networks, they offer a fascinating insight into their strengths, weaknesses, and failure modes.

In addition to adversarial samples, numerous physical attacks on neural networks have been demonstrated. Some of these attacks include patches on images that can be printed out and can fool neural networks to any desired class [7], localized noise restricted to small regions of the image outside of the central object of interest [26], trojan attacks that can act as backdoors to neural networks during test-time [33], single-pixel attacks that that can deceive smaller neural networks [52], and benign printed patterns on glasses to fool facial recognition systems [45].

Most works on generating adversarial samples and physical attacks on neural networks utilize gradient-based optimization to successfully find adversarial samples. However, gradient-based optimization attacks are only possible when attackers have full knowledge of the neural network architecture and its parameters. Thus, these methods are only applicable in the *white-box* setting, where an attacker is given full access and control over a targeted neural network. However, when targeting real-world systems such as neural networks found in autonomous vehicles or surveillance systems, attackers must operate within a *black-box* setting, in which their knowledge and access to the network is limited. In such a scenario, attackers do not have any information about the network parameters, architecture and weights, and realistically only have access to the input-output pairs of the neural network. Additionally, in numerous threat scenarios, attackers rarely have the ability to modify the entire field of view of a vision system, and are restricted to apply their attack to only small regions within the field of view. In such a threat model, attackers can thus only manipulate a small fraction of pixels of the image.

A popular approach to black-box attacks on neural networks involve white-box attacks on substitute models and hoping the generated examples transfer to the target model, such as those proposed by Papernot et al. [39]. However, this approach assumes that adversarial samples can transfer across neural networks, which is not necessarily true. It also suffers from the high computational cost required to train the substitute neural network. Recent works [11] have used finite difference

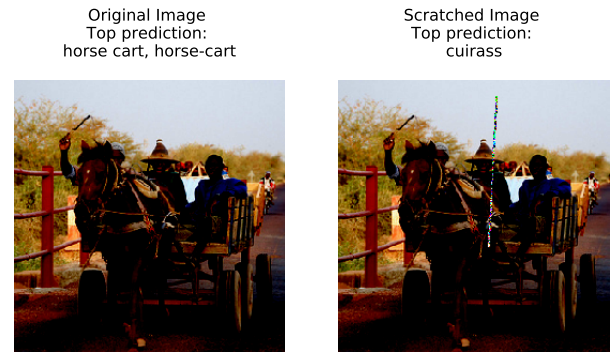
methods to directly estimate the gradients from the confidence scores, which is unfortunately very computationally expensive. Both of these approaches are query-intensive, and thus are limited in their practicality to real-world networks.

Several other works seek to tackle this issue, in which attackers utilize gradient-free optimization procedures to estimate the gradients required to fool neural networks. Such works have used Natural Evolution Strategies [25] and genetic algorithms [2] as a substitute for gradient-based optimization. One of the most popular techniques by Chen et al. [11] requires hundreds of thousands of queries to the target model, which is highly time consuming and impractical in real-world scenarios.

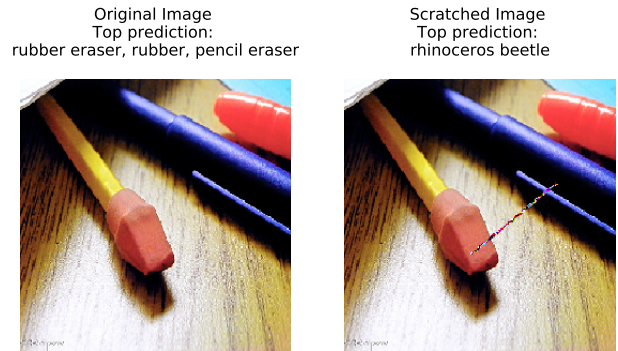
Another large constraint on most adversarial samples is that most attacks modify the *entire image* and change most of the pixels. This might not be possible for an adversary who wishes to modify only a pre-selected number of pixels in an image in the form of a line (such as a scratch on a camera sensor) or in the form of a sticker or a patch. Several works approach this problem by utilizing perturbations in the form of large patches [7] and noise outside the main image features [26]. However, such attacks are white-box and require access to the parameters and architecture of the network. Attacks such as the single-pixel attack [52] and particle swarm-optimization-based attacks [38] modify small regions of the image using black-box attacks, but they evolve the pixel location simultaneously with the pixel value and do not keep the attacked pixel locations fixed.

Motivated by the above problem, we propose *Adversarial Scratches*, a novel black-box physical attack on neural networks that manipulates highly localized regions of an image to deceive neural networks. Our method only utilizes input-output pairs of the neural network and is agnostic to the network’s architecture, parameters, and weights. To achieve gradient-free optimization, we utilize the popular Covariance Matrix Adaptation Evolutionary Strategy (CMA-ES), a gradient-free optimization technique, to iteratively find scratch values for a fixed set of pixels that can fool a neural network. We generate a custom fitness function that the CMA-ES solver uses to search for solutions effectively in a high dimensional space, and iteratively evolve populations of candidates and filter them based on their fitness until we obtain a solution that can effectively deceive the neural network.

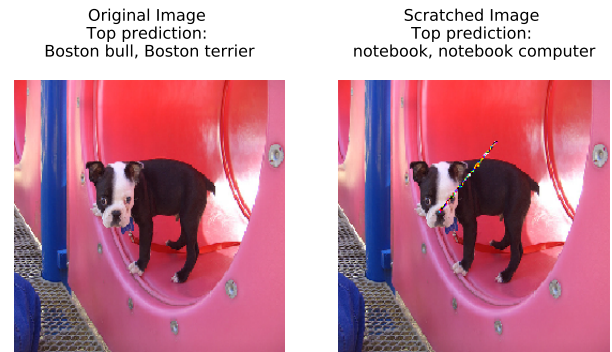
We demonstrate that *adversarial scratches* are a highly effective attack against state-of-the-art neural-network image classifiers trained on the ImageNet dataset. We achieve deceiving rates of 75.8%, 62.7%, and 45% on the Inception-v3 [53], ResNet-50 [22], and VGG-19 [51] models respectively, for images with randomly chosen scratch locations that may be fully on the object within the image, partially on the object within the image, or fully outside the object within the image. We achieve fewer queries than several existing black-box adversarial attack methods, while modifying less than 5% of the entire pixel space. Figure 1 shows examples of such noised images that are misclassified by the Inception-v3, ResNet-50, and VGG-19 networks.



(a) Scratch attack on Inception-v3



(b) Scratch attack on ResNet-50



(c) Scratch attack on VGG-19

Fig. 1. Adversarial Scratch Attack on Inception-v3, ResNet-50 and VGG-19 models.

In summary, we make the following contributions:

- We introduce *Adversarial Scratches*, a novel gradient-free approach to generate localized adversarial noise for state-of-the-art image classifiers. To the best of our knowledge, a black-box, localized attack on neural networks has not been done before. Our implementation and dataset of adversarial scratches is open-sourced to promote further research in attacking neural networks.
- We show that in the black-box setting, we require far fewer queries to attack neural networks than several other black-box attacks on neural networks.
- We empirically explore the dependence of the scratch

location for successful vs. failed attacks in terms of proximity to the object within the image.

- We demonstrate a new threat scenario for neural networks, in which adversaries are limited to black-box attacks on highly constrained regions of the image.

II. BACKGROUND

A. Supervised Learning

Supervised Machine Learning techniques involve taking labeled data and producing a classifier or regressor that can accurately predict the labels of data that the classifier has not seen before. Supervised Learning algorithms try to minimize a loss function defined for a specific problem. For classification problems, the loss function typically used is the cross-entropy loss. More formally, for a given training set D consisting of n points x with n labels y , we can define a classification problem as learning the parameters θ of a model that minimizes the following loss function loss function:

$$\sum_{i=0}^n L(f(x_i; \theta), y_i) + \Omega(\theta)$$

$L(f(x_i; \theta), y_i)$ is the loss function for each of the points x_i with label y_i that minimizes the error of prediction made by the classifier $f(\cdot)$. It is calculated as follows:

$$L(f(x_i; \theta), y_i) = \sum_{i=0}^n y_i \log(f(x_i; \theta))$$

$\Omega(\theta)$ is a regularization term independent of the training data that avoids overfitting. Supervised Learning Algorithms such as Support Vector Machines [43], Boosted Models [16], Random Forests [6], and Deep Neural Networks [17] can be depicted by this framework.

1) *Image classification*: The problem of image classification involves categorizing images into classes or labels based on the pixel content of the image. Formally, we define an image classifier as the following function:

$$f : \mathbb{R}^n \rightarrow [0, 1]^d \quad (1)$$

where d is the dimensionality of output classes and n is the number of features of the input. $f(x)_i$ represents the probability that image x corresponds to class i . Images are represented as $x \in [0, 1]^{w.h.c}$, where w, h, c are the width, height, and number of channels of the image and $n = w.h.c$. We denote the classification of the network as $c(x) = \arg \max_i f(x)_i$, with $c^*(x)$ representing the true class, or the ground truth of the image.

Traditional image-classification methods such as SIFT (Scale Invariant Feature Transform) [34] attempted to find features or pixels of the image that were invariant to scaling by a difference of Gaussians. Supervised image classification algorithms are typically trained on a labeled training set and evaluated on a held-out pre-labeled test set. Some image examples of pre-labeled image datasets are:

- The ImageNet Large Scale Visual Recognition Challenge Dataset (ILSVRC) [12], which consists of 1.2 million images with 1,000 categories, and 150,000 test and validation images.

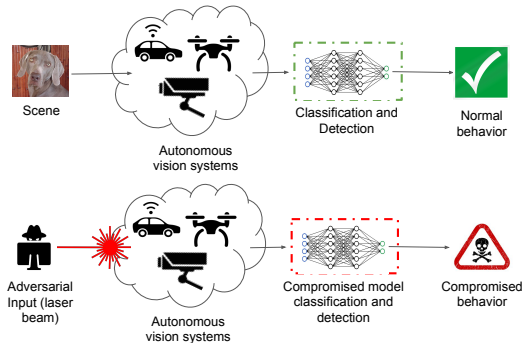


Fig. 2. Threat scenario of physical attacks on neural network vision systems to compromise behavior such as laser beams.

- The Canadian Institute For Advanced Research (CIFAR-10) dataset, which consists of 60,000 32x32 colour images in 10 classes, with 6,000 images per class. There are 50,000 training images and 10,000 test images.
- The MNIST [31] database of handwritten digits, which contains a training set of 60,000 training, and a test set of 10,000 test images.

2) *Deep Learning*: Neural Networks are a class of parametric classifiers that are effective at image classification. In particular, Deep Neural Networks [17], which consist of more than 1 hidden layer, have achieved remarkable success at image classification tasks. They were first demonstrated successfully on a large scale with AlexNet [28] winning the ILSVRC in 2012, have become the de-facto method in image classification. For this work, we focus on 3 specific architectures that have achieved state-of-the-art results on the ILSVRC, namely the Inception-v3 [53], ResNet-50 [22], and VGG-19 [51].

B. Adversarial Attacks on Deep Neural Nets

Physical Attacks on neural networks consist of attacking neural networks applied in real-world scenarios. Several prior works involve printing adversarial perturbations on 3-D models [4], adversarial patches [7], stickers placed on traffic signs [15], patterns printed on glasses to fool facial recognition systems [45], single pixel attacks [52], and adversarial stickers placed on cameras [32]. Other realistic threat scenarios, such as those depicted in Figure II-B, would involve adversaries using bright flashes or laser beams to momentarily disrupt the operation of an autonomous vehicle, drone or facial recognition system.

1) Limitations of current physical adversarial attacks:

There are several limitations to existing work on physical adversarial attacks on neural networks. Most of the attacks transferable to the real-world, such as localized adversarial noise [26], adversarial samples printed on 3-D models [4], adversarial patches [7], adversarial attacks on traffic signs [15], and adversarial stickers on cameras [32] require white-box access to the neural network, where adversaries have full access

to the neural network weights, parameters, and architecture. Of the few attacks that do utilize black-box methods, the adversarial region must either occupy a very large region of the image [7] or the location of the perturbation changes in each iteration of the adversarial attack [38], [52]. To the best of our knowledge, our method is unique in that the location of the perturbation is fixed, is generated via a black-box method, and modifies fewer than 2% of the pixels in the image. Table I depicts the different adversarial attack scenarios and where our attack method lies within them.

C. Evolutionary Strategies

Evolutionary Strategies are a class of iterative black-box optimization algorithms [55] inspired by natural evolution. At each iteration, they generate a population of candidate vectors. An objective function for each of the candidates for that population is calculated and the best performing candidates on the objective function have their parameters recombined to create the next generation of candidates. This iterative process is continued until a specified exit condition, such as a particular number of iterations or a particular fitness value is satisfied. Evolutionary Strategy algorithms differ in how they represent the populations, and how they perform mutation and recombination.

For our particular problem, which involves a black-box adversarial attack on neural networks, evolutionary strategies play a key role. In our implementation, the scratch is modeled as a 1-D vector of floating point values. For a scratch covering k pixels, we concatenate the scratch values for each of the R,G, and B color channels to obtain a vector of size $3k$ in length, whose values we iteratively evolve using the CMA-ES method.

D. CMA-ES

The most popular Evolutionary Strategy is the Covariance Matrix Adaptation Evolutionary Strategy Algorithm [21], which represents the population as the full covariance matrix multivariate Gaussian. CMA-ES has demonstrated remarkable success in solving optimization problems in low to medium dimensions. In our experimental setup, for a scratch covering m pixels, we evolve a $3m$ -long mean vector μ that keeps track of the mean values for each of the pixels in the scratch and a $3m \times 3m$ -sized covariance matrix C that tracks the pairwise dependencies between each of the pixels in the scratch. At each iteration ($t + 1$), we update the covariance matrix C^t and the mean vector μ^t , and sample P candidates from the covariance matrix and mean vector. We refer the reader to Section IV-C for a mathematically rigorous description of how the parameters are updated for each generation.

III. THREAT MODEL

We consider a threat model in which the adversary does not have access to the network architecture, parameters or training data. The attacker can solely query the target model as the black-box function outlined in Equation 1.

Formally, we consider a neural network $f(\cdot)$ used for classification where $f(x)_i$ represents the probability that image x corresponds to class i . Images are represented as $x \in [0, 1]^{w.h.c}$, where w, h, c are the width, height and number of channels of the image. We denote the classification of the network as $c(x) = \arg \max_i f(x)_i$, with $c^*(x)$ representing the true class, or the ground truth of the image. The goal of the adversary is to produce an adversarial sample x' such that it satisfies the following properties:

- The modified pixels of x are limited to only a certain region of the image. In other words, adversaries can only modify pixels of the input image x along a pre-specified line. The indices of the image adversaries are allowed to modify are denoted as *scratchLocation*.
- $c(x') \neq c^*(x)$. This means that the prediction on the adversarial sample is incorrect.

For our particular attack, we propose a unique threat model that is similar to two existing works, namely GenAttack [2] and LaVAN [26]. Our attack is similar to GenAttack in that adversaries have access solely to the prediction vector y . However, unlike GenAttack, we let the adversarial input x' take on any value in \mathbb{R}^n and do not restrict the size of perturbation added to the image, while restricting the location of perturbation on the image to a continuous scratch specified by *scratchLocation*.

In that regard, our attack is similar to the network domain as specified in LaVAN, in which adversarial patch values are restricted to certain regions, but can take any values in \mathbb{R}^n . However, it is different from LaVAN in that adversaries do not have access to the model parameters and architecture to calculate the gradient.

IV. METHODOLOGY

A. Algorithm

Adversarial Scratches relies on evolutionary strategies, which are population-based gradient-free optimization strategies. They are roughly inspired by the process of natural selection, wherein a population P of candidate solutions is generated at each iteration, termed a *generation*. Candidate solutions are evaluated using a *fitness function*, and "fitter" solutions are more likely to be selected to breed the next generation of solutions. The next generation is generated through a combination of *Crossover* and *Mutation*. Crossover involves taking numerous parent solutions, combining their parameters, and generating a new generation of solutions, similar to biological reproduction. Mutation involves applying small random perturbations to population members to increase the diversity of population members and provide a better exploration of the search space. Figure IV-A outlines the steps involved in generating adversarial scratches at a high level.

Leveraging the framework outlined by Ha [19], we can use an evolutionary strategy *solver* to solve any optimization problem as outlined in Algorithm 1.

Algorithm 2 describes the operation of generating adversarial scratches using the above framework. The inputs are the

TABLE I
ADVERSARIAL THREAT SCENARIOS FOR NEURAL NETWORKS

| | Modify all pixels | Modify a portion of the pixels | |
|-----------|--|---|-----------------------------------|
| | | Variable Perturbation Location | Fixed Perturbation Location |
| White Box | Carlini-Wagner [8], PGD [36], DeepFool [37], FGSM [54] | JSMA [40] | LaVAN [26], Adversarial Patch [7] |
| Black Box | GenAttack [2], NES attack [25] | Single Pixel Attack [52], AdversarialPSO [38] | Ours |

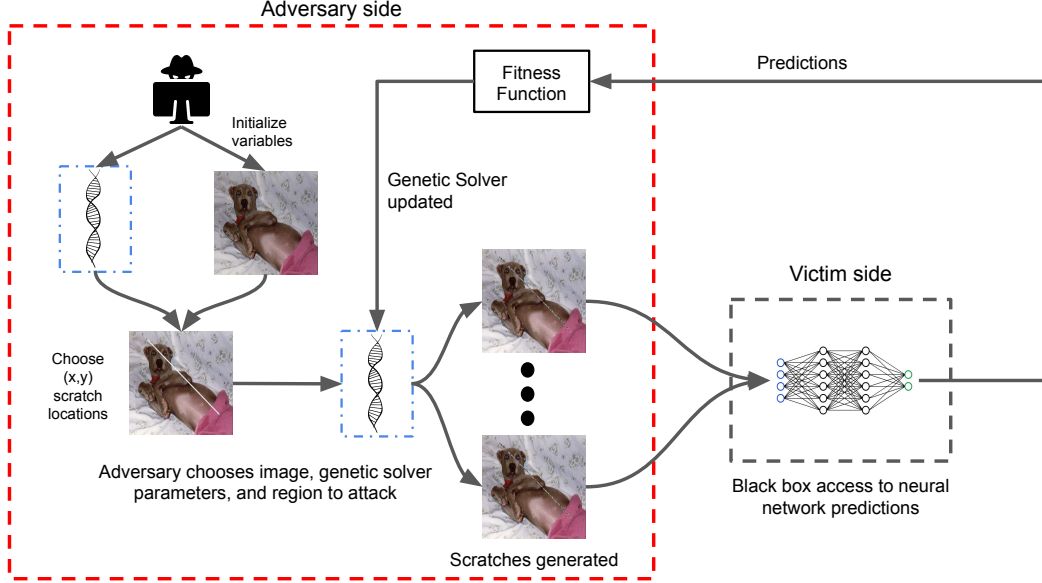


Fig. 3. General framework to generate adversarial scratches. The adversary initializes the solver parameters, target class, and region to perturb on image, then iteratively generates candidates, performs inference on the victim model, calculates the fitness of candidates, updates the solver, and repeats until the top class is the target class or the solver runs out of tries.

Algorithm 1 Framework for solving optimization problems with evolutionary strategies

Require: N , $solver$, $REQUIRED_FITNESS$

```

while True do
    // Ask Solver to give us set of solution candidates
    solutions = solver.ask()
    // Create array to hold fitness values
    fitness_list = zeros(N)
    // Calculate Fitness for each candidate
    for i = 0 to N do
        fitness_list[i] = fitness_function(solutions[i])
    end for
    // Return fitness values back to solver
    solver.tell(fitness_list)
    // get best parameter and fitness
    best_solution, best_fitness = solver.result()
    if best_fitness > REQUIRED_FITNESS then
        return best_solution
    end if
end while

```

original image img , the target model $model$, the target label $target$, the top prediction on the original image $originalPred$, the x, y coordinates for the start (x_0, y_0) and end (x_1, y_1) of the scratch, and the black-box evolutionary strategy algorithm defined as $solver$.

Algorithm 2 computes an adversarial sample $scratched_image$ by only modifying the pixels in the scratch region specified by the 2-D line drawn between (x_0, y_0) and (x_1, y_1) on the image, with $(0, 0)$ as the top-left pixel of the image. At each generation gen , Algorithm 2 initializes a population of N candidates around the current scratched image, and calculates the fitness of each of the candidates by calling $fitness_function$, whose operation is described in Algorithm 3. The solver is then passed $fitness_list$ containing the fitness of each candidate, and the best solution according to the fitness function is chosen. This process is repeated until the top prediction of the scratched image is the target class.

B. Fitness Function

The fitness function evaluates the fitness or the quality of each population member. A reasonable choice for the fitness function would be to directly maximize the probability

Algorithm 2 Calculate the Adversarial Scratch with CMA-ES

Require: $(x_0, y_0, x_1, y_1, N, GENS, img, model, target, originalPred, solver)$

```

// 1. Load in the parameters for the CMA-ES solver
solver ← N
scratched_img = img
scratchLocation = getLine((x0, y0, x1, y1))
// 2. Iterate over each generation
gen = 0
while gen ≤ GENS do
  fitness_list = zeros(N)
  // 3. Ask the solver for N solutions
  solutions = solver.ask()
  // 4. Calculate fitness of each candidate
  for i = 0 to N do
    fitness_list[i] = fitness_function(model, x0,
    y0, x1, y1, scratched_img, originalPred, target,
    solutions[i])
  // 5. Give the list of fitnesses back to the solver
  solver.tell(fitness_list)
  // 6. Obtain the best candidate and fitness from that
  generation
  best_solution, best_fitness = solver.result()
  // 7. Quit if the best candidate's prediction is the target
  class
  scratched_img[scratchLocation] = best_solution
  if model.TopPrediction(scratched_image) ==
  target then
    return scratched_image
  else
    continue
  end if
end for
end while

```

of prediction of the target class. However, in practice, we observed that jointly maximizing the target class probability and minimizing the top prediction class on the original image improved the convergence of Algorithm 2. We also observed that using a weighted logarithm of the predicted probabilities improved numerical stability. Here, α and β are weights to help with convergence. After performing a grid search of different values for α and β to optimize for the number of queries, we observed that $\alpha = 5$ and $\beta = 1$ gave the best performance in terms of query efficiency for our experimental setup.

C. CMA-ES

We utilize the popular Covariance Matrix Adaptation Evolutionary Strategy (CMA-ES) as our method of generating solution candidates for the scratch values. CMA-ES is a stochastic, derivative-free method for numerical optimization of non-convex or non-linear optimization problems. To solve an optimization problem with n variables, CMA-ES generates new solutions by sampling from a multivariate normal

Algorithm 3 Calculate the fitness for a particular solution candidate.

Require: $(model, x_0, y_0, x_1, y_1, scratched_img, originalPred, target, solution)$

```

// Obtain the region of the scratch
scratchLocation = getLine((x0, y0, x1, y1))
// Fill in the scratch
scratched_img[scratchLocation] = solution
// Predict modified image
predictions = model.predict(scratched_img)
// Return calculated fitness
targetProb = predictions[target]
originalProb = predictions[originalPred]
return alog(targetProb) - blog(originalProb)

```

distribution in \mathbb{R}^n . For our particular implementation, with a scratch covering m pixels on the image, the adversarial scratch values can be written as a vector of $n = 3m$ normal variables $X = (X_1, X_2, \dots, X_n)$ following a distribution $N(\mu, \Sigma)$, with a n dimensional mean vector μ and a $n \times n$ covariance matrix Σ . The parameters (μ, Σ) are updated every generation ($g+1$) using the parents from the previous generation g .

In particular, CMA-ES obeys the following algorithm for a mean vector μ , a covariance matrix C , evolution paths p_c and p_σ , and step size σ_k :

Algorithm 4 Covariance-Matrix Adaptation Algorithm

Require: λ // Population per generation (80 in our case)

```

// 1. Initialize variables
μ = 0, σ = 0, p_σ = 0, p_c = 0, C = 0.5
while not terminate do
  for i = 1 to λ do
    x_i = sample_from_N(μ, σ^2 C)
    f_i = fitness_function(x_i)
  end for
  x_{1...λ} = x_{s(1)...s(λ)} with s(i) = argsort(f_{1...λ}, i)
  μ' = μ
  μ ← update_means(x_1, ..., x_n)
  p_σ = update_ps(p_sigma, σ^{-1} C^{-1/2} (m - m'))
  p_c = update_pc(p_c, σ^{-1} (m - m'), ||p_σ||)
  C = update_c(C, p_c, (x_1 - m')/σ, ..., (x_λ - m')/σ)
  σ = update_sigma(σ, ||p_σ||)
  return m or x_1
end while

```

For Algorithm 4, the steps above are the following:

- $sample_from_N(\mu, \sigma^2 C)$ involves sampling from the multivariate Gaussian distribution $N(\mu, \sigma^2 C)$
- $fitness_function(x_i)$ involves calculating fitness of each of the populations using Algorithm 3.
- $update_means(x_1, \dots, x_n)$ involves updating the mean vector via a mean average of all the samples.

$$\mu^{(g+1)} = \sum_{n=0}^k w_n x_{1:\lambda}^{(g+1)}$$

Here, $(g+1)$ denotes the next generation, and w_i and $k \leq \lambda$ are weights and the number of selected points

chosen so as to obtain a weighted average of selected points .

- $update_ps(p_{sigma}, \sigma^{-1}C^{-1/2}(m - m'))$ involves updating the isotropic evolution path. It is calculated as:

$$p_sigma = (1 - c_\sigma)p_\sigma + \sqrt{c_\sigma(2 - c_\sigma)\mu_{eff}}C^{-1/2}\mu^{(g+1)}$$

with $\mu_{eff} = (\sum_{n=1}^{\mu} w_i)^{-1}$

- $update_pc(p_c, \sigma^{-1}(m - m'), \|\|p_\sigma\|\|)$ involves updating the anisotropic evolution path as:

$$p_c = (1 - c_c)p_c + h_\sigma\sqrt{c_c(2 - c_c)\mu_{eff}}\mu^{(g+1)}$$

with the learning rate $c_c \leq 1$

- $update_c(C, p_c, (x_1 - m')/\sigma, \dots, (x_\lambda - m')/\sigma)$ updates the covariance matrix C as:

$$C^{(g+1)} = (1 - c_{cov})C^g + c_{cov}/\mu_{cov} + p_cp_c^T + c_{cov}(1 - 1/\mu_{cov}) \times \sum_{n=1}^k w_i(x_1 - m')/\sigma((x_1 - m')/\sigma)^T$$

with c_{cov} generally chosen to be $\min(\mu_{cov}, \mu_{eff}, n^2)/n^2$

- $update_sigma(\sigma, \|\|p_\sigma\|\|)$ updates the step-size as:

$$\sigma = \sigma \times \exp\left(\frac{c_\sigma}{d_\sigma} \frac{(\|\|p_\sigma\|\|)}{(E\|\|N(0,1)\|\|) - 1}\right)$$

We refer the reader to Hansen’s work [21] for further details on the implementation of CMA-ES.

V. RESULTS

A. Experimental Setup

We evaluated our *Adversarial Scratches* attack method against three popular DNN image classifiers, namely the Inception-v3 [53], ResNet-50 [22] and the VGG-19 [51] models. For each of the models, we randomly chose 100 images from the ImageNet validation dataset. For each of the randomly chosen images, we chose a target class and 10 random (x_0, y_0, x_1, y_1) points that specify the location of the scratch on the image, for a total of 1000 images for each of the models.

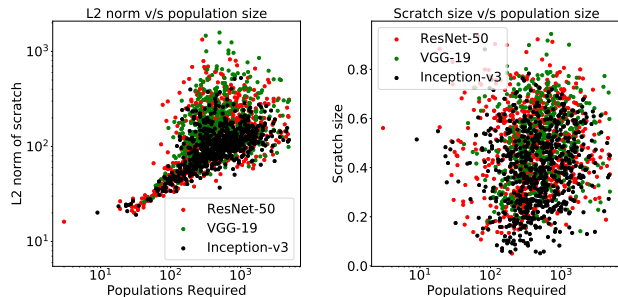
For each of the scratched images, we use a CMA-ES solver with the covariance initialized to 0.5 and dimensionality equal to the number of pixels in the scratch. The solver generated a population of 80 solution candidates for each generation, and was run until the top prediction of the scratched image was equal to the target class, or until 5,000 generations elapsed.

B. Behavior of classifiers

In our threat model, we allowed the scratch values to not be restricted to values between 0 and 1, which is typically outside the range of what is traditionally allowed for images, which might lead to large l_2 norm for the scratch, which we measure in Table II.

For each of the models, we attacked 100 randomly chosen images, each with 10 randomly chosen scratch locations. We define the fooling rate as the ratio of the number of successful attacks to the total number of attack attempts. We explore the dependence between the l_2 norm and number of populations, and the scratch size (in terms of fraction of number of pixels for the scratch relative to total number of image pixels) required for a successful attack in Figures 4a and 4b.

We observe that the fitness of the solver, and the softmax target and ground truth probability converge steadily for successfully scratched images. Several examples of this converging behavior are presented in Figure 5.



(a) l_2 norm dependence on populations of CMA-ES (b) Scratch size dependence on populations of CMA-ES

Fig. 4. Dependence of l_2 norm and scratch size (in terms of fraction of total pixels of image) on population size.

TABLE II
 l_2 NORM FOR SUCCESSFUL SCRATCHES FOR EACH OF THE MODELS.

| Model | Mean l_2 norm of scratch |
|--------------|----------------------------|
| Inception-v3 | 111.944 |
| ResNet-50 | 165.01 |
| VGG-19 | 214.78 |

C. Distribution of Successful Scratch Locations

We sought to investigate the location of scratches for successfully scratched images. In other words, we sought to answer the question: *Where should a scratch be placed on an image to fool a neural network classifier successfully?* In order to answer the question, we performed the following steps:

- Find the features of the input image that contribute most to the neural network predictions for a particular class;
- Threshold the pixels to obtain a bounding box for pixels that contribute most to a class;
- Observe the intersection of the pixels of the scratch and the pixels of the bounding box of the most relevant features.

To find the features of the input image that contribute most to a particular ground truth class, we utilized the Grad-CAM tool [44], which is a visualization tool for neural networks that generates heatmaps of the pixels that contribute most to a particular class. It achieves this by calculating the gradient of the top predicted class y with respect to the feature maps of the last convolutional layer A^k , and then globally pooling them to obtain the neuron importance, which is then applied to the input.

After generating the heatmaps using Grad-CAM, we thresholded the images on their red channels to within 80% of the red pixel values to obtain bounding boxes that denote the limits of the relevant features for a particular class. To determine the location of the scratch relative to the relevant ground-truth features we found the ratio of pixels of the scratch inside the bounding box. Table III demonstrates our results for this experiment.

We observed that, on average, for the Inception-v3, ResNet-50, and VGG-19 models, 34.89%, 22.47% and 39.25% of

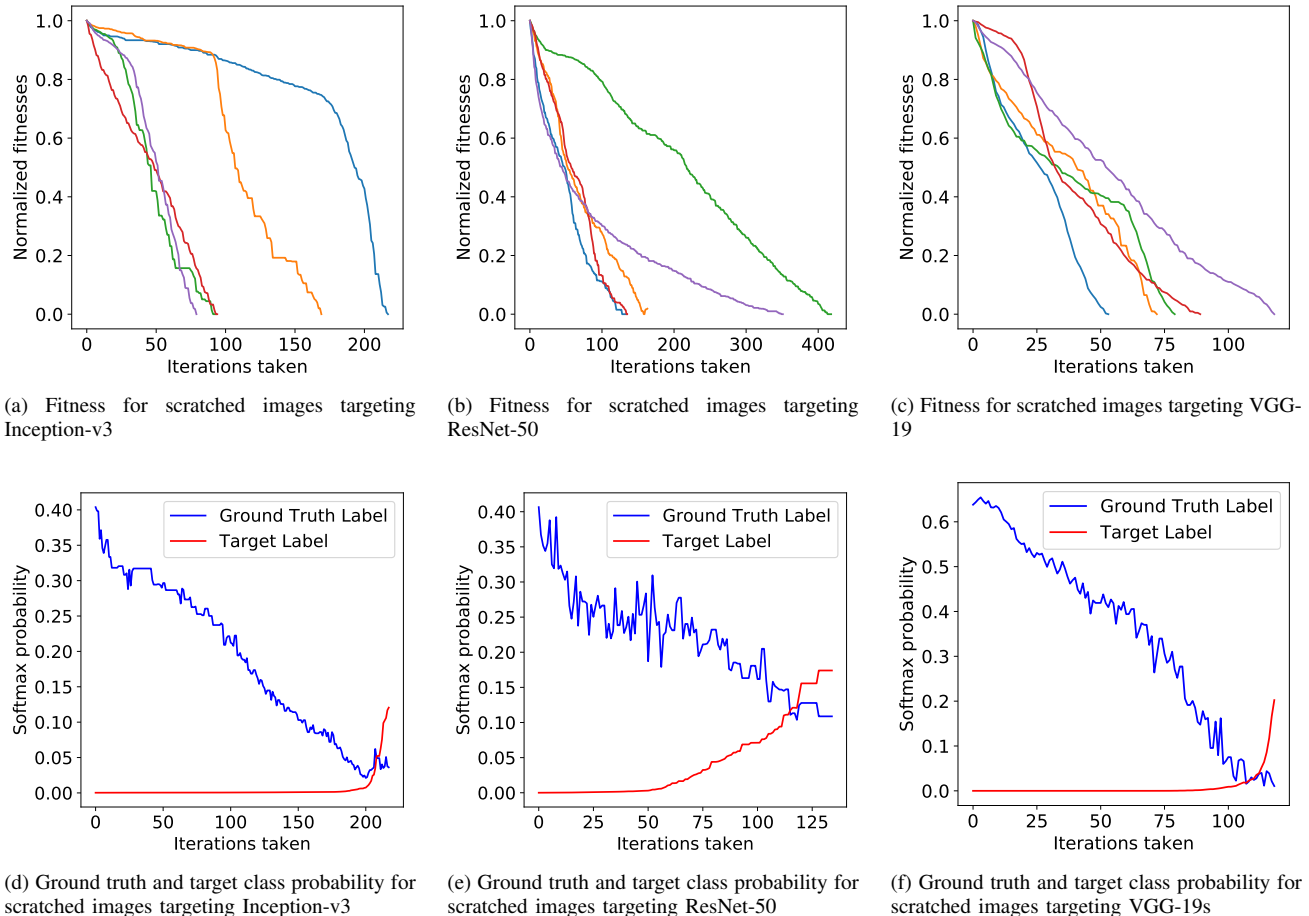


Fig. 5. Convergence of fitness and softmax target class probability for successfully scratched images targeting Inception-v3, ResNet-50 and VGG-19.

TABLE III
FRACTIONS OF SCRATCHES FOUND INSIDE AND OUTSIDE BOUNDING BOXES GENERATED BY GRADCAM.

| | Inception-v3 | ResNet50 | VGG19 |
|--|--------------|----------|--------|
| Average fraction of scratch pixels within box | 33.97% | 36.22% | 24.09% |
| Average fraction of scratches outside box | 34.89% | 22.47% | 39.25% |
| Convolutional layer used for feature extraction | Mixed_7c | layer4 | relu_3 |

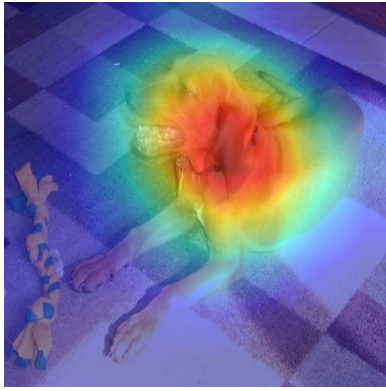
the scratches were not on the main features contributing to the ground truth class and could be placed in any arbitrary region of the image. Of the scratches that were part of the main contributing features, 33.97%, 36.22%, and 24.09%, respectively of the scratch pixels were present on the main contributing features of the image. This further elucidates the possibility of real-world attacks on neural networks, where the adversarial noise need not cover the entire image and can be restricted to a very small region of the image that need not be on the object detected by the neural network. Figure 6 shows some examples of successfully scratched images, where the locations of the adversarial scratches were outside of the main

features relevant to the ground truth of the image.

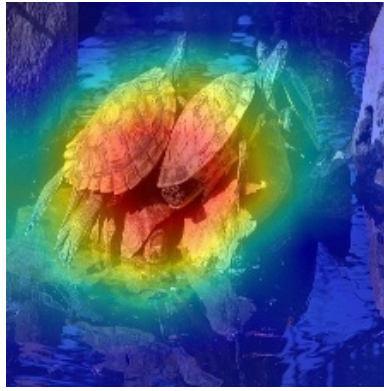
D. Query Performance

Our threat model is unique in that adversaries can only modify select regions of the image in a black-box setting. To find a meaningful comparison against other methods with respect to the number of queries required and fooling rate, we compare our method against state-of-the-art black-box adversarial attacks in which adversaries are allowed to modify the entire image on the models they were evaluated on. These attacks are GenAttack [2], ZOO [11], and Natural Evolution Strategies (NES) [25]. Additionally, we compare the fooling rates of our method against other methods for the models they were evaluated on. Figure 7 shows the distribution of queries required to achieve successful attacks for each of the neural network models, and Table V shows the queries required to generate successful attacks for each of the models. Table V shows that both the mean and median number of queries required to generate successful attacks depends on the number of parameters.

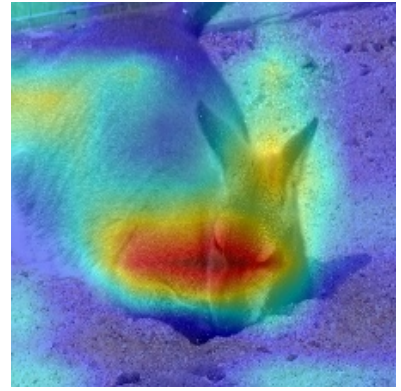
The mean query efficiencies for the different black-box attacks on an Inception-v3 model are compared in Table IV.



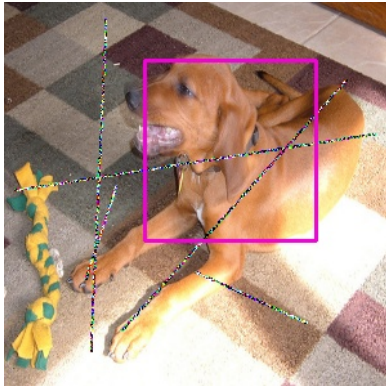
(a) Grad-CAM heatmap for image correctly classified by Inception-v3



(b) Grad-CAM heatmap for image correctly classified by ResNet-50



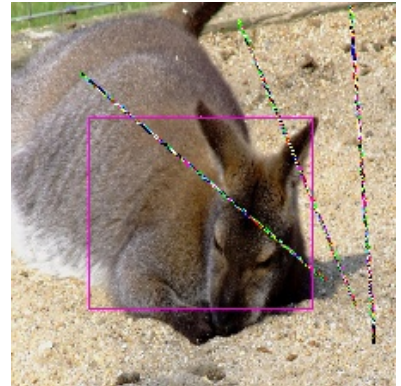
(c) Grad-CAM heatmap for image correctly classified by VGG-19



(d) Successful scratches on image targeting Inception-v3



(e) Successful scratches on image targeting ResNet-50



(f) Successful scratches on image targeting VGG-19

Fig. 6. Location of scratches relevant to heatmap of the features that contribute most to the ground truth of the image.

We outperform 2 out of 4 state-of-the-art black-box attack methods.

TABLE IV
COMPARISON OF QUERIES REQUIRED FOR SUCCESSFUL ATTACKS ON INCEPTION-V3

| Attack method | Mean queries |
|--------------------|--------------|
| GenAttack baseline | 97,493 |
| GenAttack | 11,081 |
| ZOO | 2,611,456 |
| NES | 14,737 |
| Ours | 35,600 |

TABLE V
QUERIES REQUIRED FOR SUCCESSFUL ATTACKS ON DEEP NEURAL NETWORK MODELS

| Model | Median queries | Mean queries | Neural Network parameters |
|--------------|----------------|--------------|---------------------------|
| Inception-v3 | 35600 | 53902 | 23.8M |
| ResNet-50 | 32480 | 53139 | 25.6M |
| VGG-19 | 36320 | 56344 | 144M |

E. Transferability of scratches

We evaluate the transferability of the adversarial scratches, namely the predictions of Deep Neural Networks on scratches generated to fool a different network architecture. Namely, we measure the *untargeted* fooling rate, which is defined as the fraction of predictions that are not equal to the ground truth labels.

In particular, we measured the prediction accuracy for each of the 100 randomly chosen ImageNet validation images we chose to scratch. For 50 of the correctly classified images, we added an adversarial scratch targeting one network, then measured the prediction of several other networks on that scratched image. For this experiment, we generated 50 scratches for both of ResNet-50 and VGG-19, and measured the predictions of Inception-v3, ResNet-18 [22], SqueezeNet [24], ResNet-50, VGG-19, VGG-16, ResNet-34, VGG-13, DenseNet-201 [23], ResNet-152, ResNet-101, VGG-11, and AlexNet [28] on each of the scratched images. The untargeted fooling rates are shown in Table VI.

F. Limitations

Our method is not without limitations and might be applied to only certain environments. As demonstrated in Section V-D,

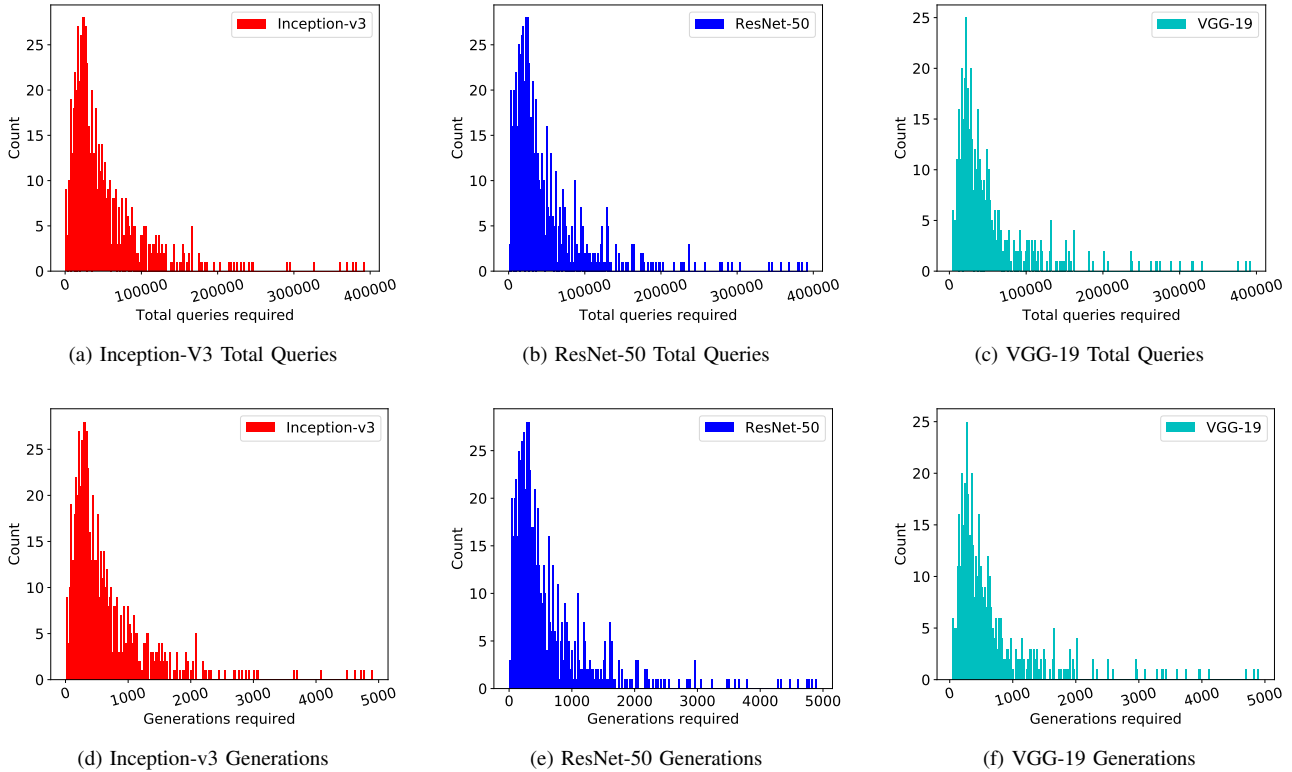


Fig. 7. The distribution of the queries and generations required for successful attacks on Inception-v3, ResNet-50 and VGG-19 neural network models.

TABLE VI
GENERALIZABILITY OF ADVERSARIAL SCRATCHES ACROSS DIFFERENT NETWORKS. PERCENTAGES INDICATE UNTARGETED FOOLING RATES. COLUMNS INDICATE ARCHITECTURE FOR WHICH THE SCRATCHES WERE COMPUTED, AND ROWS INDICATE ARCHITECTURE FOR WHICH FOOLING RATE IS REPORTED.

| | Generated for | |
|----------------------|---------------|--------|
| | ResNet-50 | VGG-19 |
| Inception-v3 | 66% | 60% |
| SqueezeNet1_0 | 80% | 88% |
| SqueezeNet1_1 | 90% | 92% |
| VGG-11 | 66% | 78% |
| VGG-13 | 60% | 68% |
| VGG-16 | 56% | 46% |
| VGG-19 | 62% | 100% |
| ResNet-18 | 32% | 44% |
| ResNet-34 | 32% | 44% |
| ResNet-50 | 100% | 44% |
| ResNet-101 | 26% | 30% |
| ResNet-152 | 26% | 36% |
| densenet201 | 20% | 28% |
| AlexNet | 82% | 80% |

we require a significant number of queries on the target models to launch a successful attack. Additionally, the attack method is limited in that successful attacks require very large perturbations on the scratch pixels, thereby limiting attack

scenarios to where attackers must create pixel values outside the dynamic range available for sensors, such as shining very bright lasers.

VI. RELATED WORK

In this section, we explore related work in the white-box, black-box, and physical attacks on neural networks with respect to full-view attacks (where attackers can modify all the image pixel values) and partial-view attacks (where attackers only modify few pixel values).

A. White-Box Attacks

1) *Full image attacks.*: In white-box scenarios, attackers have access to all information about the target model, such as its architecture and weights. The adversaries utilize back-propagation to compute gradients, by which they can craft adversarial samples that can deceive neural networks. Most works focus on adding small amounts of noise across the entire image, which is imperceptible to the human eye. We briefly summarize some of these works below:

- *L-BFGS.* L-BFGS [54] uses box-constrained L-BFGS to minimize the l_2 norm of the added adversarial noise $\|\delta\|_2$ subject to the $f(x + \delta) = t$, where t is the target class and the neural network is defined using Equation 1.
- *FGSM and I-FGSM.* Goodfellow et al. [18] propose the Fast Gradient Sign method (FGSM) to rapidly generate adversarial samples. For a given l_{inf} constraint ϵ , the attack utilises the sign of the gradient loss J with respect

to the input x and true label y to generate an adversarial sample x_{adv} as:

$$x_{adv} = x + \epsilon \times \text{sign}(\nabla J(x, l)).$$

Targeted attacks can be launched by computing the loss with respect to a target t and going in the direction of the negative gradient. I-FGSM [29] is an iterative version of FGSM that uses a finer distortion constant and clips the l_{inf} value. In PGD, or projected gradient descent, I-FGSM is performed with random starts, and has been shown to be a powerful first-order adversarial attack.

- *Carlini-Wagner and EAD*. Carlini-Wagner l_2 attack [8] utilizes the logit layer to craft adversarial samples with an L_2 regularized loss function. By handling the box constraint $x \in [0, 1]^n$ with a change of variables, they used Adam to minimize the following function:

$$c \times f(x, t) + \|x_{\text{adversarial}} - x\|_2^2.$$

where c is a prespecified constant and $f(x, t)$ is a loss function that depends on the logit layer values and the target class t . EAD [10] is a generalization of this attack and uses an additional l_1 penalty. It has been shown to generate more robust and transferable adversarial samples [35], [46], [47].

2) *Limited field of view attacks*.: In several white-box attacks, adversaries might choose to not add noise to the entire image, but rather might add noise to localized regions of an image. Some of these works are summarized below.

- *Adversarial Glasses*. Sharif et al. [45] were able to deceive neural network-based facial recognition systems by adding specially reconstructed frame textures to glasses by utilizing particle-swarm optimization.
- *Physical Attacks against Neural Networks*. Evtimov et al. [15] caused misclassification of traffic signs by neural networks by applying specific patterns to real-world objects. In particular, given a neural network according to Equation 1, they seek to find a perturbation δ on the mask of an image x such that $f(x + \delta) = t$, where t is a target class that is different from the ground truth of the image x .
- *Localized Adversarial Noise*. Karmon et al. [26] were able to generate highly localized noise for a state-of-the-art Inception-v3 neural network trained on ImageNet. Their method is similar to the one proposed by Eykholt et al. [15] in that the perturbations are localized in small regions of the image and are restricted to only a few pixels. However, their implementation is different as they allowed the pixel values to choose any value and did not restrict them to lie between 0 and 1.
- *Adversarial Patches*. Brown et al. [7] were able to generate printable patches that are immune to scaling and rotation and that can be used for physical attacks. In particular, they trained to optimize a patch over a number of images, transformations of the patch, and distribution over locations in the image.

B. Black-Box Attacks

In black-box scenarios, attackers typically have access only to the input-output pairs. Implementations of such attacks typically utilize non-gradient based methods of optimization, such as evolutionary strategies or genetic algorithms. We summarize some of these works below:

- *GenAttack*. Alzantot et al. [2] use a genetic algorithm to minimize the l_{∞} norm of the added adversarial noise $\|\delta\|_{\infty}$ subject to the $f(x + \delta) = t$, while simultaneously maximizing the fitness function $\text{fitness}(x) = \log(f(x)_t) - \log(\sum(f(x)_c))$ where t is the target class, c is the set of all classes excluding the target class, and the neural network is defined according to Equation 1. At each iteration they evolve a set of candidates N , evaluate the fitness of the candidates, and use their parameters to generate the next set of candidates.
- *Natural Evolution Strategies Attack*. Ilyas et al. [25] use Natural Evolutionary Strategies in a similar manner to GenAttack [2] to attack an Inception-v3 model under multiple threat scenarios, namely a Query-limited setting (which is most similar to ours), a partial-information setting (where the adversary only has access to top-k labels) and the label-only setting, where the adversary only has access to the labels and not the confidence values. In their work they attack an Inception-v3 model and the commercially available Google Cloud Vision API.
- *AdversarialPSO*. Mosli et al. [38] use Particle Swarm Optimization, a population based gradient-free optimization algorithm, to attack neural network classifiers trained on the CIFAR-10, MNIST and ImageNet datasets, in which they evolve the locations as well as the pixel values through their evolutionary algorithm.

All of the mentioned black-box attacks either attack the entire image or choose pixels to modify, based on their sensitivity to the outputs. Our attack is different in that we attack only a small, restricted region of the image consisting of less than 5% of total pixels of the image, while restricting our attack region to a randomly chosen scratch or line along the image.

C. Gradient-Free Optimization for Black-Box attacks

Deep learning’s success comes largely from its ability to efficiently calculate gradients of an objective for each model parameter, which allows for searching over a large parameter space to find a solution.

Evolutionary Strategies have emerged as an alternative to gradient-based methods where it might not be possible to directly utilize the gradients or model parameters. They are roughly inspired by the process of natural selection, wherein a population P of candidate solutions is generated at each iteration, termed a *generation*. Candidate solutions are evaluated using a *fitness function*, and “fitter” solutions are more likely to be selected to breed the next generation of solutions. We outline several popular evolutionary strategies below.

- **Genetic Algorithms.** Genetic Algorithms are among the most popular black-box optimization methods. In general, solutions for an n dimensional real-valued solution vector x are modeled as a multivariate Gaussian distribution parametrized by its mean vector μ and standard deviations σ with a probability distribution $N(\mu, \sigma^2 I)$. The key difference between this and the CMA-ES method is that only the diagonal elements of the covariance matrix are updated. For each generation, a fraction λ of the population P is kept and their parameters are recombined to generate samples for the next generation as follows:

$$\mu^{t+1} = \frac{1}{(\lambda P)} \sum_{i=1}^{i=\lambda P} x_i^{(t+1)} \quad (2)$$

$$\sigma^{(t+1)2} = \frac{1}{\lambda P} \sum_{i=1}^{i=\lambda P} (x_i^{(i+1)} - \mu^t)^2 \quad (3)$$

Due to the lack of diversity in the subsequent generations most genetic algorithms tend to converge to a local optimum of the objective function. GenAttack [2] utilizes genetic algorithms to generate adversarial noise for CIFAR-10 and MNIST image classifiers.

- **Covariance Matrix Adaptation Evolutionary Strategy (CMA-ES).** The CMA-ES method adapts for the μ and σ parameters of the parent generation by sampling from the entire covariance matrix of the parameter space. At each generation, the covariance matrix is updated by the parameters the fittest samples of that particular population, and is sampled from to generate candidates for subsequent generations. We explain the implementation of CMA-ES in further detail in Section IV-C.
- **Natural Evolution Strategies (NES).** (NES) [58] seeks to optimize in the search distribution space. In particular, NES works with a probability distribution space characterized by $(\theta, p_\theta(x))$; it looks for the steepest direction within a small step in the distribution space, where the distance is measured by the KL divergence, which is computed by a Taylor expansion. The fitness associated with one sample x is labeled as $f(x)$ and the search distribution over θ is parameterized by θ . It is calculated as:

$$J(\theta) = \mathbb{E}_{p_\theta(x)}[f(x)] = \int_x f(x) p_\theta(x) dx \quad (4)$$

Using the log-likelihood trick, the gradient of the fitness can be calculated as follows:

$$\begin{aligned} \nabla_\theta J(\theta) &= \nabla_\theta \int_x f(x) p_\theta(x) dx \\ &= \int_x f(x) \frac{p_\theta(x)}{p_\theta(x)} \nabla_\theta p_\theta(x) dx \\ &= \int_x f(x) p_\theta(x) \nabla_\theta \log p_\theta(x) dx \\ &= \mathbb{E}_{p_\theta(x)}[f(x) \nabla_\theta \log p_\theta(x)] \end{aligned} \quad (5)$$

- **Particle Swarm Optimization** Particle Swarm Optimization, originally proposed by Kennedy and Eberhart [27], is a gradient-free, black-box optimization algorithm that has been applied in numerous realistic scenarios, such as text feature selection, grid job scheduling and generating adversarial samples for neural networks. The algorithm works by dispersing particles in a search space and moving them around till a solution or exit condition is reached; the location of the particle with the best fitness is the solution vector. For a n -dimensional problem space, an n -dimensional position vector x and n -dimensional velocity vector v are evolved according to the following equation at each iteration t :

$$x_i(t+1) = x_i(t) + v_i(t+1) \quad (6)$$

The velocity vector v is updated as:

$$v_i(t+1) = wv_t + c_1 r_1 (p_g - x_t(t)) + c_2 r_2 (p_i - x_i(t)) \quad (7)$$

The second equation contains three terms. The first term w controls much influence the current velocity has when calculating the next velocity. The second term is referred to as the exploration variable, and allows particles to explore regions in the direction of the best position in the swarm, denoted by p_g and is weighted by c_1 and a uniformly distributed random variable r_1 to induce stochasticity in generating the parameters. The third term constants c_2 and r_2 similarly weight and randomize the exploitation portion of search, which explores particles in the vicinity of the current particle. Subsequent implementations of PSO experiment with the weighing factors.

VII. DISCUSSION

We initially attempted to use a simple Gaussian Genetic Algorithm, where a k -dimensional scratch was modeled as a $3k$ -long real-valued vector x with the probability distribution $N(\mu, \sigma^2 I)$. The key difference between this and the CMA-ES method is that we only update the diagonal elements of the covariance matrix. At each iteration t , we sampled $P = 50$ candidates $x_{i=1:50}$ and recombined the parameters according to Equation 2 and 3, with λ being chosen as 25%.

We quickly discovered that this method would consistently get stuck in local minima and was not effective as an attack; hence, we decided to use CMA-ES as an alternative due to its ability to incorporate larger diversity in generating descendant populations via off-diagonal elements of the covariance matrix.

For our constrained threat scenario (limited queries, black-box attack, limited field of view), we discovered that the overwhelming majority of scratch values were outside the dynamic range allowed for images, i.e., outside the range $[0, 1]$. A physical implementation of such an attack might involve physical malfunctioning of the camera sensors or pixels, where the camera pixel outputs values outside the dynamic range of $[0, 1]$, or oversaturation of the camera's gain, such as shining

a bright light or a laser beam at a camera as depicted in Figure IV-A.

A potential defense against such an attack would be to implement *physical* safeguards in camera hardware and software before deployment of autonomous systems, such as ensuring rapid automatic gain control (AGC) in the camera gain mechanisms, securing the camera sensors from physical manipulations that could override their behavior, and ensuring software checks to prevent images from exceeding their dynamic range.

VIII. CONCLUSIONS

In this work, we propose a new threat scenario for neural networks, in which adversaries have access solely to the predictions and are limited in their ability to modify the entire input. We propose a new attack, called *adversarial scratches*, which is successful in this highly constrained threat scenario against state-of-the-art deep neural network image classifiers.

For future work, we intend to apply other gradient-free optimization techniques to generate adversarial scratches and explore methods of generating adversarial scratches with values restricted within the dynamic range of the images. Additionally, we plan to explore the equivalent of adversarial scratches for speech recognition systems, such as chirped sequences that appear benign, but might potentially be malicious.

REFERENCES

- [1] S. Albarqouni, C. Baur, F. Achilles, V. Belagiannis, S. Demirci, and N. Navab, "Agnet: deep learning from crowds for mitosis detection in breast cancer histology images," *IEEE transactions on medical imaging*, vol. 35, no. 5, pp. 1313–1321, 2016.
- [2] M. Alzantot, Y. Sharma, S. Chakraborty, and M. Srivastava, "Genat-tack: Practical black-box attacks with gradient-free optimization," *arXiv preprint arXiv:1805.11090*, 2018.
- [3] M. Alzantot, Y. Sharma, A. Elgohary, B.-J. Ho, M. Srivastava, and K.-W. Chang, "Generating natural language adversarial examples," *arXiv preprint arXiv:1804.07998*, 2018.
- [4] A. Athalye, L. Engstrom, A. Ilyas, and K. Kwok, "Synthesizing robust adversarial examples," *arXiv preprint arXiv:1707.07397*, 2017.
- [5] T. Bansal, J. Pachocki, S. Sidor, I. Sutskever, and I. Mordatch, "Emergent complexity via multi-agent competition," *arXiv preprint arXiv:1710.03748*, 2017.
- [6] L. Breiman, "Random forests," *Machine learning*, vol. 45, no. 1, pp. 5–32, 2001.
- [7] T. B. Brown, D. Mané, A. Roy, M. Abadi, and J. Gilmer, "Adversarial patch," *arXiv preprint arXiv:1712.09665*, 2017.
- [8] N. Carlini and D. Wagner, "Towards evaluating the robustness of neural networks," in *2017 IEEE Symposium on Security and Privacy (SP)*. IEEE, 2017, pp. 39–57.
- [9] —, "Audio adversarial examples: Targeted attacks on speech-to-text," in *2018 IEEE Security and Privacy Workshops (SPW)*. IEEE, 2018, pp. 1–7.
- [10] P.-Y. Chen, Y. Sharma, H. Zhang, J. Yi, and C.-J. Hsieh, "Ead: elastic-net attacks to deep neural networks via adversarial examples," in *Thirty-second AAAI conference on artificial intelligence*, 2018.
- [11] P.-Y. Chen, H. Zhang, Y. Sharma, J. Yi, and C.-J. Hsieh, "Zoo: Zeroth order optimization based black-box attacks to deep neural networks without training substitute models," in *Proceedings of the 10th ACM Workshop on Artificial Intelligence and Security*. ACM, 2017, pp. 15–26.
- [12] J. Deng, W. Dong, R. Socher, L.-J. Li, K. Li, and L. Fei-Fei, "Imagenet: A large-scale hierarchical image database," in *2009 IEEE conference on computer vision and pattern recognition*. Ieee, 2009, pp. 248–255.
- [13] J. Devlin, M.-W. Chang, K. Lee, and K. Toutanova, "Bert: Pre-training of deep bidirectional transformers for language understanding," *arXiv preprint arXiv:1810.04805*, 2018.
- [14] S. Edunov, M. Ott, M. Auli, and D. Grangier, "Understanding back-translation at scale," *arXiv preprint arXiv:1808.09381*, 2018.
- [15] K. Eykholt, I. Evtimov, E. Fernandes, B. Li, A. Rahmati, C. Xiao, A. Prakash, T. Kohno, and D. Song, "Robust physical-world attacks on deep learning models," *arXiv preprint arXiv:1707.08945*, 2017.
- [16] Y. Freund and R. Schapire, "A short introduction to boosting," *Journal-Japanese Society For Artificial Intelligence*, vol. 14, no. 771-780, p. 1612, 1999.
- [17] I. Goodfellow, Y. Bengio, and A. Courville, *Deep learning*, 2016.
- [18] I. J. Goodfellow, J. Shlens, and C. Szegedy, "Explaining and harnessing adversarial examples," *arXiv preprint arXiv:1412.6572*, 2014.
- [19] D. Ha, "A visual guide to evolution strategies," November 2019. [Online]. Available: <http://blog.otoro.net/2017/10/29/visual-evolution-strategies/>
- [20] A. Hannun, C. Case, J. Casper, B. Catanzaro, G. Diamos, E. Elsen, R. Prenger, S. Satheesh, S. Sengupta, A. Coates *et al.*, "Deep speech: Scaling up end-to-end speech recognition," *arXiv preprint arXiv:1412.5567*, 2014.
- [21] N. Hansen, "The cma evolution strategy: A tutorial," *arXiv preprint arXiv:1604.00772*, 2016.
- [22] K. He, X. Zhang, S. Ren, and J. Sun, "Deep residual learning for image recognition," in *Proceedings of the IEEE conference on computer vision and pattern recognition*, 2016, pp. 770–778.
- [23] G. Huang, Z. Liu, L. Van Der Maaten, and K. Q. Weinberger, "Densely connected convolutional networks," in *Proceedings of the IEEE conference on computer vision and pattern recognition*, 2017, pp. 4700–4708.
- [24] F. N. Iandola, S. Han, M. W. Moskewicz, K. Ashraf, W. J. Dally, and K. Keutzer, "Squeezenet: Alexnet-level accuracy with 50x fewer parameters and 0.5 mb model size," *arXiv preprint arXiv:1602.07360*, 2016.
- [25] A. Ilyas, L. Engstrom, A. Athalye, and J. Lin, "Black-box adversarial attacks with limited queries and information," *arXiv preprint arXiv:1804.08598*, 2018.
- [26] D. Karmon, D. Zoran, and Y. Goldberg, "Lavan: Localized and visible adversarial noise," *arXiv preprint arXiv:1801.02608*, 2018.
- [27] J. Kennedy, "Particle swarm optimization," *Encyclopedia of machine learning*, pp. 760–766, 2010.
- [28] A. Krizhevsky, I. Sutskever, and G. E. Hinton, "Imagenet classification with deep convolutional neural networks," in *Advances in neural information processing systems*, 2012, pp. 1097–1105.
- [29] A. Kurakin, I. Goodfellow, and S. Bengio, "Adversarial examples in the physical world," *arXiv preprint arXiv:1607.02533*, 2016.
- [30] Q. Le, O. Boydell, B. Mac Namee, and M. Scanlon, "Deep learning at the shallow end: Malware classification for non-domain experts," *Digital Investigation*, vol. 26, pp. S118–S126, 2018.
- [31] Y. LeCun and C. Cortes, "MNIST handwritten digit database," 2010. [Online]. Available: <http://yann.lecun.com/exdb/mnist/>
- [32] J. B. Li, F. R. Schmidt, and J. Z. Kolter, "Adversarial camera stickers: A physical camera attack on deep learning classifier," *arXiv preprint arXiv:1904.00759*, 2019.
- [33] Y. Liu, S. Ma, Y. Aafer, W.-C. Lee, J. Zhai, W. Wang, and X. Zhang, "Trojaning attack on neural networks," 2017.
- [34] D. G. Lowe, "Distinctive image features from scale-invariant keypoints," *International journal of computer vision*, vol. 60, no. 2, pp. 91–110, 2004.
- [35] P.-H. Lu, P.-Y. Chen, K.-C. Chen, and C.-M. Yu, "On the limitation of magnet defense against l1-based adversarial examples," in *2018 48th Annual IEEE/IFIP International Conference on Dependable Systems and Networks Workshops (DSN-W)*. IEEE, 2018, pp. 200–214.
- [36] A. Madry, A. Makelov, L. Schmidt, D. Tsipras, and A. Vladu, "Towards deep learning models resistant to adversarial attacks," in *International Conference on Learning Representations*, 2018. [Online]. Available: <https://openreview.net/forum?id=rJzIBFZAb>
- [37] S.-M. Moosavi-Dezfooli, A. Fawzi, and P. Frossard, "Deepfool: a simple and accurate method to fool deep neural networks," in *Proceedings of the IEEE conference on computer vision and pattern recognition*, 2016, pp. 2574–2582.
- [38] R. Mosli, M. Wright, B. Yuan, and Y. Pan, "They might not be giants: Crafting black-box adversarial examples with fewer queries using particle swarm optimization," *arXiv preprint arXiv:1909.07490*, 2019.

- [39] N. Papernot, P. McDaniel, I. Goodfellow, S. Jha, Z. B. Celik, and A. Swami, "Practical black-box attacks against machine learning," in *Proceedings of the 2017 ACM on Asia conference on computer and communications security*. ACM, 2017, pp. 506–519.
- [40] N. Papernot, P. McDaniel, S. Jha, M. Fredrikson, Z. B. Celik, and A. Swami, "The limitations of deep learning in adversarial settings," in *2016 IEEE European Symposium on Security and Privacy (EuroS&P)*. IEEE, 2016, pp. 372–387.
- [41] A. Radford, J. Wu, R. Child, D. Luan, D. Amodei, and I. Sutskever, "Language models are unsupervised multitask learners."
- [42] E. Raff, J. Barker, J. Sylvester, R. Brandon, B. Catanzaro, and C. K. Nicholas, "Malware detection by eating a whole exe," in *Workshops at the Thirty-Second AAAI Conference on Artificial Intelligence*, 2018.
- [43] B. Scholkopf and A. J. Smola, *Learning with kernels: support vector machines, regularization, optimization, and beyond*, 2001.
- [44] R. R. Selvaraju, M. Cogswell, A. Das, R. Vedantam, D. Parikh, and D. Batra, "Grad-cam: Visual explanations from deep networks via gradient-based localization," in *Proceedings of the IEEE International Conference on Computer Vision*, 2017, pp. 618–626.
- [45] M. Sharif, S. Bhagavatula, L. Bauer, and M. K. Reiter, "Accessorize to a crime: Real and stealthy attacks on state-of-the-art face recognition," in *Proceedings of the 2016 ACM SIGSAC Conference on Computer and Communications Security*. ACM, 2016, pp. 1528–1540.
- [46] Y. Sharma and P.-Y. Chen, "Attacking the madry defense model with l_1 -based adversarial examples," *arXiv preprint arXiv:1710.10733*, 2017.
- [47] —, "Bypassing feature squeezing by increasing adversary strength," *arXiv preprint arXiv:1803.09868*, 2018.
- [48] W. Shen, M. Zhou, F. Yang, C. Yang, and J. Tian, "Multi-scale convolutional neural networks for lung nodule classification," in *International Conference on Information Processing in Medical Imaging*. Springer, 2015, pp. 588–599.
- [49] D. Silver, A. Huang, C. J. Maddison, A. Guez, L. Sifre, G. Van Den Driessche, J. Schrittwieser, I. Antonoglou, V. Panneershelvam, M. Lanctot *et al.*, "Mastering the game of go with deep neural networks and tree search," *nature*, vol. 529, no. 7587, p. 484, 2016.
- [50] D. Silver, T. Hubert, J. Schrittwieser, I. Antonoglou, M. Lai, A. Guez, M. Lanctot, L. Sifre, D. Kumaran, T. Graepel *et al.*, "Mastering chess and shogi by self-play with a general reinforcement learning algorithm," *arXiv preprint arXiv:1712.01815*, 2017.
- [51] K. Simonyan and A. Zisserman, "Very deep convolutional networks for large-scale image recognition," *arXiv preprint arXiv:1409.1556*, 2014.
- [52] J. Su, D. V. Vargas, and K. Sakurai, "One pixel attack for fooling deep neural networks," *IEEE Transactions on Evolutionary Computation*, 2019.
- [53] C. Szegedy, V. Vanhoucke, S. Ioffe, J. Shlens, and Z. Wojna, "Rethinking the inception architecture for computer vision," in *Proceedings of the IEEE conference on computer vision and pattern recognition*, 2016, pp. 2818–2826.
- [54] C. Szegedy, W. Zaremba, I. Sutskever, J. Bruna, D. Erhan, I. Goodfellow, and R. Fergus, "Intriguing properties of neural networks," *arXiv preprint arXiv:1312.6199*, 2013.
- [55] W. Vent, "Rechenberg, ingo, evolutionsstrategieoptimierung technischer systeme nach prinzipien der biologischen evolution. 170 s. mit 36 abb. frommann-holzboog-verlag. stuttgart 1973. broschiert," *Feddes Repertorium*, vol. 86, no. 5, pp. 337–337, 1975.
- [56] R. Vinayakumar, M. Alazab, K. Soman, P. Poornachandran, and S. Venkatraman, "Robust intelligent malware detection using deep learning," *IEEE Access*, vol. 7, pp. 46717–46738, 2019.
- [57] O. Vinyals, I. Babuschkin, W. M. Czarnecki, M. Mathieu, A. Dudzik, J. Chung, D. H. Choi, R. Powell, T. Ewalds, P. Georgiev *et al.*, "Grandmaster level in starcraft ii using multi-agent reinforcement learning," *Nature*, pp. 1–5, 2019.
- [58] D. Wierstra, T. Schaul, T. Glasmachers, Y. Sun, J. Peters, and J. Schmidhuber, "Natural evolution strategies," *The Journal of Machine Learning Research*, vol. 15, no. 1, pp. 949–980, 2014.